eIRxIV EMERGING INVESTIGATORS PREPRINT SERVER

June 9, 2026

Analyzing the efficiency of aircraft using biomimetic wings

Madhav S Anoop[1], Anoop Krishnan[2]

[1] Round Rock High School, Round Rock, TX, US

[2] Round Rock High School, Round Rock, TX, US

Student Authors
Madhav S Anoop, High School

SUMMARY

Air transportation significantly worsens global climate change by emitting roughly 1 billion tons of carbon dioxide annually, highlighting a critical need for innovative solutions. This study focused on designing more efficient aircraft wings to minimize drag and optimize energy utilization. We hypothesized that aircraft with biomimetically inspired wings would experience lower drag, thereby increasing the lift-to-drag ratio, improving fuel efficiency, and reducing carbon emissions. We conducted a two-phased study to design and test biomimetic wings inspired by eagle wings and humpback whale tubercles. In Phase 1, Computational Fluid Dynamics (CFD) simulations and wind-tunnel testings on 10-inch wing models demonstrated that the whale-mimetic wing's lift-to-drag ratio was higher than the conventional wing at almost all the angles of attack and airspeeds tested, with the greatest improvement of approximately 47% observed at an angle of attack (AoA) of 5 degrees and an airspeed of 50 m/s. We eliminated the eagle-mimetic design from further studies due to its borderline performance compared to the conventional wing. Testing in a custom-built wind tunnel physically validated the improved lift of the whale-mimetic wing. Phase-2 advanced the whale-mimetic and conventional designs to 40.5-inch full-wing models. CFD simulations on these full wings consistently supported the initial findings. Finally, real-world flight testing utilizing a custom-built commercial drone-sized prototype revealed that the whale-mimetic wing achieved an approximately 12% increase in flight distance per volt of battery consumed compared to the conventional wing.

This preprint reports new research that has not
been peer-reviewed and revised at the time of posting.

CC BY

INTRODUCTION

Air transportation significantly worsens global climate change by emitting roughly 1 billion tons of carbon dioxide annually, highlighting a critical need for innovative solutions (1). The aviation industry is growing very rapidly, and more aircraft are being flown. In fact, according to the International Air Transportation Association, air travel by passengers is up 10.4% in 2024 compared to 2023. This is up 3.8% compared to pre-pandemic conditions (2). This illustrates how the aviation industry is rapidly expanding, hence the resulting carbon emissions are also increasing significantly.

Scientists have linked rising global temperatures to an increase in the frequency and severity of extreme weather events, accelerating sea-level rise, and disruptions to ecosystems (3). Mitigating these severe impacts requires immediate reductions in CO2 emissions across all industrial sectors (4).

To reduce the aviation industry's carbon emissions, we focused on improving the efficiency of the aircraft wings.

The two main factors affecting the performance of an aerofoil are lift and drag. Lift is created by two factors: first, the aerofoil deflects air downward. According to Newton's third law, the fast-moving air exerts an equal and opposite force on the aerofoil, generating lift. Second, due to the curved shape at the top of the aerofoil, the air travels faster on the top than on the flat bottom. The faster-moving air on the top has lower pressure than the slower-moving air at the bottom of the aerofoil, which pushes the aerofoil upwards, generating lift (5). There are two types of drag on an aerofoil: induced drag, which is directly related to the amount of lift created, and pressure drag, which is caused by the shape of an object and how air separates from its surface, creating a turbulent wake (6, 7, 8). We aimed to reduce both these types of drag on the aerofoil by designing bio-mimetic aerofoils.

We chose to mimic an eagle's primary feathers and a humpback whale’s (Megaptera novaeangliae) tubercles (Figure 1) to reduce the drag on the aerofoil (9, 10). Primary feathers on an eagle's wing reduce wingtip vortices by acting like "slots" at the wingtip, spreading out the swirling air created by the wing's lift. Essentially, the separated feathers at the wingtip break up the large vortex into smaller, less impactful ones (11, 12). The whale tubercles disrupt the water flow, causing small, rotating fluid columns to form along the surface, which act as miniature

This preprint reports new research that has not
been peer-reviewed and revised at the time of posting.

CC BY

vortex generators. These vortices mix high-momentum fluid from the free stream with the slower boundary layer flow. This mixing increases the momentum of the boundary layer, allowing it to follow the wing's curvature more easily and thus reducing flow separation and improving the lift-to-drag ratio (13, 14, 15, 16, 17).

We hypothesized that the aircraft using biomimetically inspired wings would incur less drag, thereby increasing the lift-to-drag ratio, resulting in improved fuel efficiency and reduced carbon emissions. Through a two-phase research approach, we first evaluated small wing models before advancing to full-wing models and real-world flight testing. Whale-mimetic CFD simulations demonstrated a consistent and significant improvement in the lift-to-drag ratio over conventional aerofoils. Wind-tunnel testing results were consistent with the performance observed in CFD simulations. Finally, real-world flight testing with a custom-built prototype aircraft validated these findings, demonstrating an increase in flight distance per volt of battery consumed. Ultimately, this project demonstrated the viability of adapting whale tubercles into aircraft wing designs to improve an aircraft's efficiency, resulting in reduced fuel consumption and carbon emissions.

RESULTS

To verify how the biomimetic wings performed compared to conventional wings, we conducted three types of tests. We conducted Computational Fluid Dynamics (CFD) simulations and custom-built wind-tunnel testing to compare performance under controlled, ideal conditions. Subsequently, we conducted flight testing using a custom-built, commercial drone-sized prototype aircraft to validate the aerodynamic performance and energy efficiency under real-world conditions.

Computational Fluid Dynamics (CFD)

To understand how the biomimetic wings performed compared to conventional wings, we calculated the lift-to-drag ratio for three wing designs: whale-mimetic, eagle-mimetic, and conventional. We determined this from over 15,000 Computational Fluid Dynamics (CFD) simulation trials executed at airspeeds of 50 m/s, 100 m/s, and 240 m/s at angles of attack of 0, 5, and 10 degrees. During Phase 1, these tests were executed using 10-inch-long, 4-inch-wide wing models (Figure 1).

For the whale-mimetic versus conventional lift-to-drag ratio analysis, the calculations indicated that the probability of the conventional aerofoil having a higher lift-to-drag ratio than the

This preprint reports new research that has not
been peer-reviewed and revised at the time of posting.

whale-mimetic one was significantly low ($p < 0.05$, two-sample t-test). The CFD simulation confidence interval (CI) showed that, 95% of the time, the whale-mimetic aerofoil lift-to-drag ratio was 0.9344 to 1.7542 times that of the conventional aerofoil lift-to-drag ratio (Figure 3). CFD airflow visualization confirmed the tubercles induced delayed flow separation, which drove this improvement (Figure 2).

For the eagle-mimetic versus conventional lift-to-drag ratio analysis, the probability of the conventional aerofoil outperforming the eagle-mimetic wing was considerable at 50 m/s ($p = 0.13256$, two-sample t-test). The 95% confidence interval was -0.1938 to 0.6202. Because 0 is inside the confidence interval, no significant difference between the means was observed (Figure 3).

In Phase-2, we ruled out the eagle-mimetic design and expanded CFD simulations to utilize wing models measuring 40.5 inches long and 9 inches wide for both the conventional and whale-mimetic designs (Figure 5). In Phase 2, the angles of attack of 5 and 10 degrees and the airspeeds of 10 m/s, 30 m/s, and 50 m/s were used. The whale-mimetic wing design showed a lift-to-drag ratio improvement of 14.5% at an angle of attack of 5 degrees and an airspeed of 30 m/s. It also showed a 21.23% lift-to-drag improvement at an angle of attack of 10 degrees and an airspeed of 30 m/s. At a 5° AoA and an airspeed of 10 m/s, the biomimetic wing demonstrated a significantly higher L/D ratio (Two-sample t-test, $p = 0.00049$). We can be 95% confident that the mean difference in the lift-to-drag ratio between the whale-mimetic and conventional aerofoils at an angle of attack of 5 and an airspeed of 10 m/s is from 0.2928 to 0.6935. (Figure 6). These simulations demonstrated results consistent with the Phase 1 tests and indicated an aerodynamic advantage for the whale-mimetic design.

Custom-built Wind-tunnel Testing

To physically validate CFD simulation results under controlled conditions, we built a custom wind tunnel and tested the Phase 1 whale-mimetic and conventional wing models. Since the CFD simulations demonstrated that the whale-mimetic aerofoil performed better than the eagle-mimetic and the conventional aerofoil, we compared the best-performing whale-mimetic aerofoil against the conventional aerofoil. The Phase 1 wind-tunnel testing for whale-mimetic aerofoil generated lift up to 1.51% of its weight, and the conventional aerofoil generated lift only up to 1.35% of its weight. p-value of .00000107 from a 2-sample t-test indicated that the probability of a conventional aerofoil having a higher L/D ratio than whale-mimetic is significantly

This preprint reports new research that has not
been peer-reviewed and revised at the time of posting.

CC BY

low(< 5%). Wind-tunnel testing CI showed that 95% of the time, the whale lift will be (1.4543, 2.7457) higher than the lift generated by a conventional aerofoil. Both confidence intervals did not include 0, confirming that the whale aerofoil has a statistically higher L/D ratio than the conventional airfoil (Figure 4). These results were consistent with the performances observed for the airfoils during CFD simulations.

Flight Testing and Telemetry Data

To compare the aerodynamic fuel efficiency in a real-world environment during Phase 2, a commercial drone-sized prototype aircraft with a 40.5-inch wingspan was flown using the 3D printed conventional and whale-mimetic wings. We recorded telemetry data using a custom GPS data logger. After filtering out flights shorter than 100 meters, the telemetry indicated that the prototype utilizing the conventional wing averaged a distance of 1596.90 meters per volt of battery consumed at an average speed of 9.89 m/s. Under a similar average speed, the prototype equipped with the whale-mimetic wing traveled an average of 1802.01 meters per volt. This represented an approximately 12% longer flight distance per volt of battery consumed for the whale-mimetic aerofoil (Table 1). This result was very close to the CFD simulation results of 14.5% lift-to-drag ratio improvement at an angle of attack of 5 degrees and an airspeed of 30 m/s.

DISCUSSION

Whale-mimetic wings resulted in highly efficient aerodynamic performance. Our results validated the initial hypothesis: incorporating biomimetic features found on humpback whale tubercles onto an aircraft wing reduces drag, increases the lift-to-drag ratio, and improves operational flight range.

The whale-mimetic model's Phase 1 CFD simulations showed a consistent and significant improvement in lift-to-drag ratio over the conventional aerofoil across all angles of attack and airspeeds tested. The lift-to-drag ratio gain of the whale-mimetic model was in the range of 47% at an angle of attack of 5 degrees (optimal for cruise) and an airspeed of 50 m/s (Figure 3). The significantly lower p-values for the whale models and confidence intervals without 0 support acceptance of the hypothesis regarding the whale-mimetic model. Conversely, the eagle-mimetic model showed positive results in only 50% of the tests. The variance in significance suggests that the data do not currently support the hypothesis regarding the eagle-mimetic model. For this reason, only the whale-mimetic and conventional wing designs advanced to Phase 1 custom-built wind-tunnel testing and Phase 2 testing.

This preprint reports new research that has not
been peer-reviewed and revised at the time of posting.

Wind-tunnel testing for the whale-mimetic aerofoil generated lift up to 1.51% of its weight, while the conventional aerofoil generated lift only up to 1.35% of its weight (Figure 4).

Phase-2 utilized the 40.5-inch full wing for CFD and physical flight testing to better represent the real-world aerodynamics of commercial delivery drones. Flight testing results further substantiated the aerodynamic improvements observed in the CFD and wind-tunnel experiments. The recorded telemetry data indicated an approximately 12% increase in distance covered per volt of battery consumed when utilizing the whale-mimetic wing compared to the conventional wing (Table 1). This result was very close to the CFD simulation results of 13.5% lift-to-drag ratio improvement at an angle of attack of 5 degrees and an airspeed of 10 m/s (Figure 6).

This real-world energy efficiency improvement directly translates to extended operational range and endurance for unmanned aerial vehicles. The Breguet Range equation provides an estimate of an aircraft's range under certain assumptions. The lift-to-drag ratio is in the numerator of the Breguet Range Equation, which indicates that an aircraft's range is proportional to its lift-to-drag ratio (18). We expect the ~15% increase in lift-to-drag ratio observed in the CFD simulations to yield a proportional ~15% increase in both range and endurance for a typical commercial drone, which could mathematically expand a drone's total accessible service area by approximately 32%. The service area for the drone is π(radius)squared. A 15% increase in L/D could mean approximately 15% increase in operating radius. Therefore, the new service area could be π(radius*1.15)squared, which is 1.323 times the original service area.

This area expansion would provide substantial direct operational benefits, including fewer base depots and expanding rural reach for medical logistics, increasing the monitoring coverage area per flight for agricultural inspections, and improving loiter times while reducing necessary fleet sizes for defense operations.

There are multiple limitations within this study. We could not replicate high airspeeds in the custom-built wind tunnel, generating only around 4 m/s wind. While we could measure the lift in the wind tunnel, we could not physically measure drag due to the lack of affordable instrumentation. During the flight testing, manual pilot control introduced inherent natural

This preprint reports new research that has not
been peer-reviewed and revised at the time of posting.

variability. While average speeds remained comparable, it was impossible to precisely control the flight speed throughout each trial. Additionally, while we conducted all flights when anemometer readings were at zero, we cannot entirely rule out slight environmental wind impacts. However, flying both models back-to-back on the same days using the same battery pack significantly mitigated these environmental variables. Since only 20 flights with a flight distance of more than 100 meters could be completed, a statistical data analysis could not be conducted on the flight test data.

Future work will translate these aerodynamic findings into a deployable community toolkit combining lightweight screening software, design examples, and guided instructional materials for robotics teams and maker communities.

Industry projections estimate that commercial drones will account for 800 million deliveries by the year 2030 (19, 20). Companies leading this expansion, such as Wing and Zipline, rely on battery-powered systems that will benefit immensely from drag reduction (21, 22). Applying whale-mimetic aerofoils to these drones would improve their energy efficiency, increase their range and payload capacity, and make them more adoptable. Ultimately, whale-mimetic drones can execute commercial deliveries, emitting less CO_2 and consuming less energy than standard short-distance delivery vans. This project successfully demonstrated the viability of adapting whale tubercles into aircraft wing designs to improve aircraft efficiency and reduce fuel usage.

MATERIALS AND METHODS

3D modeling wing design

Three wing designs were created using Autodesk Fusion software. A conventional cambered wing was designed and used as the control wing in the experiments. The whale-mimetic and eagle-mimetic features were added to the control wing to create test wings in the experiment. During the first phase of research, small wings measuring 10 inches in length, 4 inches in width, and 0.5 inches in height were designed. For the second phase, commercial drone-size wings measuring 40.5 inches of wingspan, 9 inches in width, and 1 inch in height were created. In the Autodesk Fusion software, the control and test wings were set up at 0, 5, and 10 degrees of angle of attack (AoA).

Computational Fluid Dynamics (CFD) simulation

Autodesk CFD was used for executing CFD simulations to measure lift and drag forces on the control and test wings. The simulations were conducted at airspeeds of 50 m/s, 100 m/s, and

This preprint reports new research that has not
been peer-reviewed and revised at the time of posting.

CC BY

240 m/s. In Phase 1, simulations were executed using one side of the wing with a 10-inch length and 4-inch width. The size, length, depth, and distribution of the biomimetic features were iteratively changed to identify the best designs. Once the optimal biomimetic wing designs were identified, 204 CFD simulations were executed, resulting in over 15,000 trials to statistically analyze the lift and drag forces on the control and test wings. In Phase-2, simulations were expanded to test the aerodynamics of the 40.5-inch full wingspan with 9-inch width. Statistical significance was determined using two-sample t-tests with an alpha value of 0.05.

Custom-built Wind-tunnel testing

A wind tunnel was built to measure the lift generated by the control wing and the whale-mimetic wing. A high-speed fan was used for wind generation. To mitigate the spinning vortex created by the fan, a honeycomb formation of 1-inch PVC pipes was constructed using over 280 6-inch pipes to force the air to turn laminar. The fan's airspeed was approximately 6 m/s, resulting in an airspeed of around 4 m/s inside the wind tunnel. The control wing and the whale-mimetic test wing were 3D printed using the Bambu Lab A1 printer. Using a precision weighing machine, the difference in weight before and after the fan was activated was calculated to measure the amount of lift generated by the control and test wings.

Prototype fabrication

In Phase-2, a prototype fuselage with 31 inches in length was constructed utilizing lightweight paper foam to ensure structural durability while minimizing weight. The conventional and whale-mimetic wings, featuring a 40.5-inch wingspan, a 9-inch chord, and 1-inch max height, were 3D printed using lightweight PLA-Aero foaming filament. To maintain structural integrity during flight, the wings were printed with internal support bridges, split into four parts due to 3D printer size limitations, and joined using hot glue and paper foam reinforcements.

Flight Telemetry Circuitry and Data Collection

The prototype aircraft was powered and controlled by an electronic speed controller, a 3S LiPo battery, and a standard transmitter and receiver system. A custom telemetry circuit was built to log the necessary telemetry data. The HGLRC M100-5883 GPS module provided location data at 10Hz via UART protocol, and the data was written to the microSD card synchronously using a high-speed SPI protocol, all controlled by an Arduino Nano 33 BLE Sense Rev2. The Arduino was programmed using the TinyGPS++ library that uses the Haversine formula to calculate flight distances. The program actively ignores positional updates representing less than 3

This preprint reports new research that has not
been peer-reviewed and revised at the time of posting.

meters of movement to prevent stationary GPS drift accumulation. Battery voltages were manually recorded before and after each flight using a 1-8S battery checker.

CONFLICTS OF INTEREST

The authors declare they have no conflicts of interest.

REFERENCES

1. *SF Group Climate Action White Paper*. SF Express, 2025, www-static.sf-express.com/uploads/2_Climate_Action_White_Paper_5f38790db1.pdf. Accessed 1 Apr 2026.

2. International Air Transport Association. "Global Air Passenger Demand Reaches Record High in 2024." *International Air Transport Association*, 30 Jan. 2025, www.iata.org/en/pressroom/2025-releases/2025-01-30-01/. Accessed 1 May 2025.

3. Intergovernmental Panel on Climate Change. "Climate Change 2023: Synthesis Report." *Intergovernmental Panel on Climate Change*, 2023, www.ipcc.ch/report/ar6/syr/. Accessed 10 May 2025.

4. "The Effects of Climate Change." *NASA Science*, 23 Oct. 2024, science.nasa.gov/climate-change/effects/. Accessed 15 May 2025.

5. "Learn about Aerodynamics." *NASA Glenn Research Center*, 7 Dec. 2023, www1.grc.nasa.gov/beginners-guide-to-aeronautics/learn-about-aerodynamics/#lift. Accessed 15 June 2024.

6. Benson, Tom. "Induced Drag Coefficient." *NASA Glenn Research Center*, www.grc.nasa.gov/www/k-12/VirtualAero/BottleRocket/airplane/induced.html. Accessed 30 June 2024.

7. Celli, Vittorio. "Boundary Layer Separation and Pressure Drag." *University of Virginia*, 28 Sept. 1997, galileo.phys.virginia.edu/classes/311/notes/fluids2/node11.html. Accessed 30 June 2024.

8. Adrian, Ronald J., et al. "Blunt Bodies." *Princeton University*, www.princeton.edu/~asmits/Bicycle_web/blunt.html. Accessed 30 June 2024.

This preprint reports new research that has not been peer-reviewed and revised at the time of posting.

CC BY

9. Tucker, V. A. "Gliding Birds: Reduction of Induced Drag by Wing Tip Slots between the Primary Feathers." *Journal of Experimental Biology*, vol. 180, no. 1, 1993, pp. 285–310, journals.biologists.com/jeb/article-abstract/180/1/285/6536/Gliding-Birds-Reduction-of-Induced-Drag-by-Wing. Accessed 10 July 2024.

10. Fish, F. E., and J. M. Battle. "Hydrodynamic Design of the Humpback Whale Flipper." *Journal of Morphology*, vol. 225, no. 1, 1995, pp. 51–60, doi.org/10.1002/jmor.1052250105. Accessed 10 July 2024.

11. "This Is How Winglets Work." *Boldmethod*, 12 Mar. 2022, www.boldmethod.com/learn-to-fly/aerodynamics/how-winglets-reduce-drag-and-how-wingtip-vortices-form/. Accessed 10 July 2024.

12. "Wingtip Vortices and Wake Turbulence." *Pilot Institute*, 28 Mar. 2025, pilotinstitute.com/wingtip-vortices/. Accessed 17 July 2025.

13. Miklosovic, D. S., et al. "Leading-Edge Tubercles Delay Stall on Humpback Whale (*Megaptera novaeangliae*) Flippers." *Physics of Fluids*, vol. 16, no. 5, 2004, pp. L39–L42, doi.org/10.1063/1.1688341. Accessed 17 July 2024.

14. Cai, C., et al. "Numerical Investigations of the Hydrodynamic Performance of Hydrofoils with Leading-Edge Protuberances." *Advances in Mechanical Engineering*, vol. 7, no. 7, 2015, doi.org/10.1177/1687814015592088. Accessed 17 July 2024.

15. Zhang, J., et al. "Numerical and Experimental Analysis of Biomimetic Tubercle for Cavitation Suppression in Viscous Oil Flow around Hydrofoil." *Engineering Applications of Computational Fluid Mechanics*, vol. 18, no. 1, 2024, doi.org/10.1080/19942060.2024.2394176. Accessed 27 July 2024.

16. "Lift-to-Drag Ratio." *NASA Glenn Research Center*, 19 Jul. 2024, www1.grc.nasa.gov/beginners-guide-to-aeronautics/lift-to-drag-ratio/. Accessed 27 July 2024.

17. Hamilton, Tyler. "Whale-Inspired Wind Turbines." *MIT Technology Review*, 6 Mar. 2008, www.technologyreview.com/2008/03/06/221447/whale-inspired-wind-turbines/. Accessed 3 Aug. 2024.

This preprint reports new research that has not been peer-reviewed and revised at the time of posting.

CC BY

18. Radovitzky, Raúl. "Unified Engineering: Materials and Structures: Breguet Range Equation." *MIT OpenCourseWare*, 2021, ocw.mit.edu/courses/16-001-unified-engineering-materials-and-structures-fall-2021/mit16_001_f21_lec_driver_art.pdf. Accessed 7 June 2025.

19. Stolaroff, J. K., et al. "Energy Use and Life Cycle Greenhouse Gas Emissions of Drones for Commercial Package Delivery." *Nature Communications*, vol. 9, no. 1, 2018, article no. 409, doi.org/10.1038/s41467-017-02411-5. Accessed 7 June 2025.

20. "The Future of the Last-Mile Ecosystem." *World Economic Forum*, 10 Jan. 2020, www.weforum.org/publications/the-future-of-the-last-mile-ecosystem/. Accessed 12 July 2025.

21. *Wing*, wing.com/. Accessed 17 Aug. 2024.

22. *Zipline*, www.flyzipline.com/. Accessed 6 Sept. 2025.

FIGURES AND TABLES

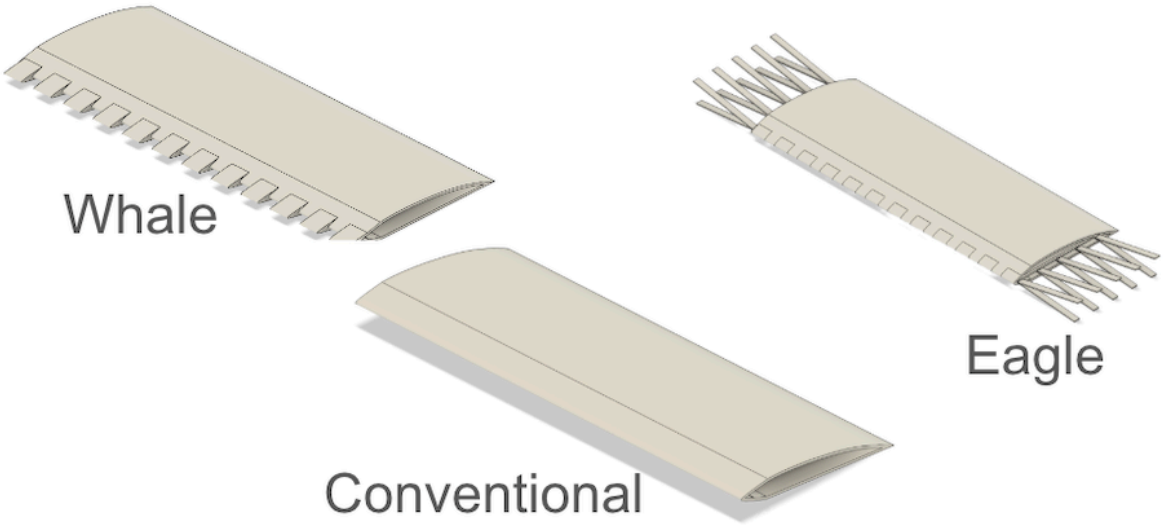

Figure 1. 3D CAD models of the three Phase 1 wing designs. (A) The conventional Clark-Y control wing. (B) The whale-mimetic wing incorporating tubercles on the leading edge. (C) The eagle-mimetic wing features slotted primary feathers. These designs were evaluated in Phase 1 simulations and tests.

This preprint reports new research that has not been peer-reviewed and revised at the time of posting.

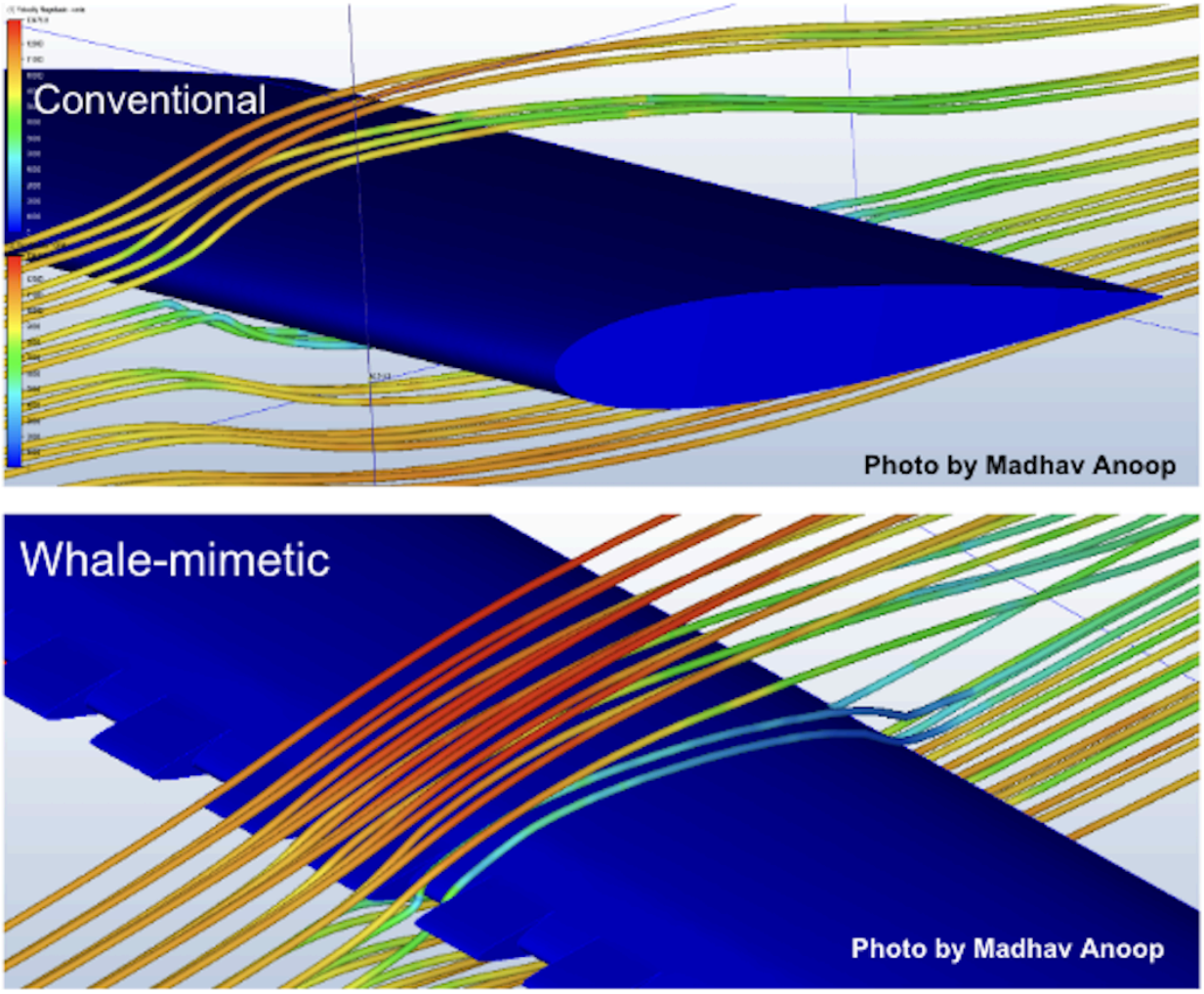

Figure 2. CFD airflow visualization demonstrating delayed flow separation on a whale-mimetic wing. This is a cross-section of a whale-mimetic wing and a conventional wing, showing the airflow around them. The airflow visually illustrates the delayed flow separation above the whale-mimetic wing compared to the Conventional wing.

This preprint reports new research that has not
been peer-reviewed and revised at the time of posting.

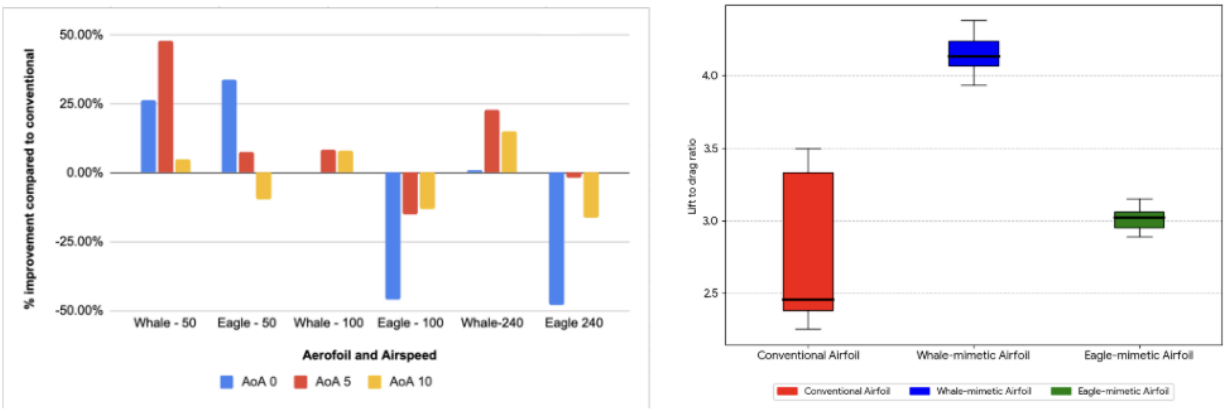

Figure 3. Improvement in lift-to-drag ratio derived from Phase 1 CFD simulations on 10-inch wing models. (A) The bar chart data shows the percentage improvement in the L/D ratio relative to the conventional control wing (n=204). The improvement consistently peaks for the whale-mimetic design, reaching approximately 47% at a 5-degree AoA, which is optimal for cruise. In contrast, improvements to the eagle-mimetic model yielded positive results in only some trials, supporting the decision to eliminate the eagle design. (B) Boxplots illustrate the distribution of experimental L/D ratios among the control Cambered wing (Conventional Airfoil) and test Whale and Eagle mimetic wings at an AoA of 5 degrees and the airspeed of 50 m/s. The horizontal line within each box indicates the median. A highly significant difference in means was observed between the Conventional and Whale designs (p-value: 0.0000203), confirming that the whale-mimetic airfoil has a statistically higher L/D ratio than the conventional airfoil. The 95% confidence interval (CI) for the mean difference (1.3443) between these groups is (0.9344, 1.7542), which does not include 0. The standard deviation for the whale-mimetic airfoil's L/D ratio is 0.1367. Analysis between the conventional and eagle-mimetic airfoils returned an insignificant p-value of 0.13256. However, the 95% CI for the mean difference between these airfoils is (-0.1938, 0.6202); as this interval includes 0, a significant difference between the means cannot be concluded, suggesting the observed difference could be due to random chance.

This preprint reports new research that has not
been peer-reviewed and revised at the time of posting.

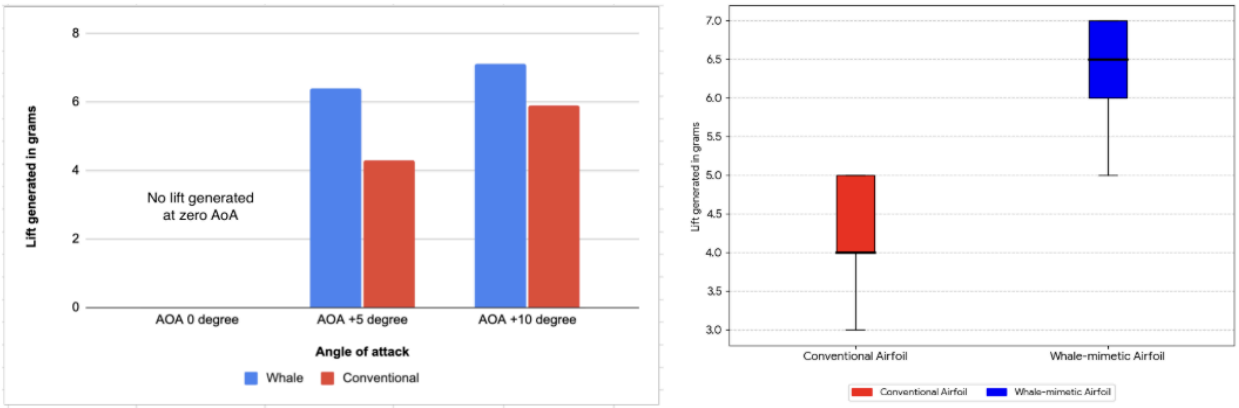

Figure 4. Physical lift comparison between conventional and whale-mimetic wings in Phase 1 Custom-built wind-tunnel testing. (A) Custom 3D-printed small 10-inch wings (conventional and whale-mimetic) were tested in controlled laminar flow conditions (n=10). The measured lift confirmed that the whale-mimetic design consistently outperforms the conventional design, with lift generation peaking around a 10-degree AoA. (B) Box plots illustrate the distribution, median, and interquartile spread of lift generated in grams from wind-tunnel testing for 3D printed cambered (conventional) and whale-mimetic wings. Whale-mimetic wing generated a significantly higher maximum lift than conventional wing ($p = 0.00000107$). The calculated mean difference was 2.1, with a 95% confidence interval of (1.4543, 2.7457).

This preprint reports new research that has not been peer-reviewed and revised at the time of posting.

CC BY

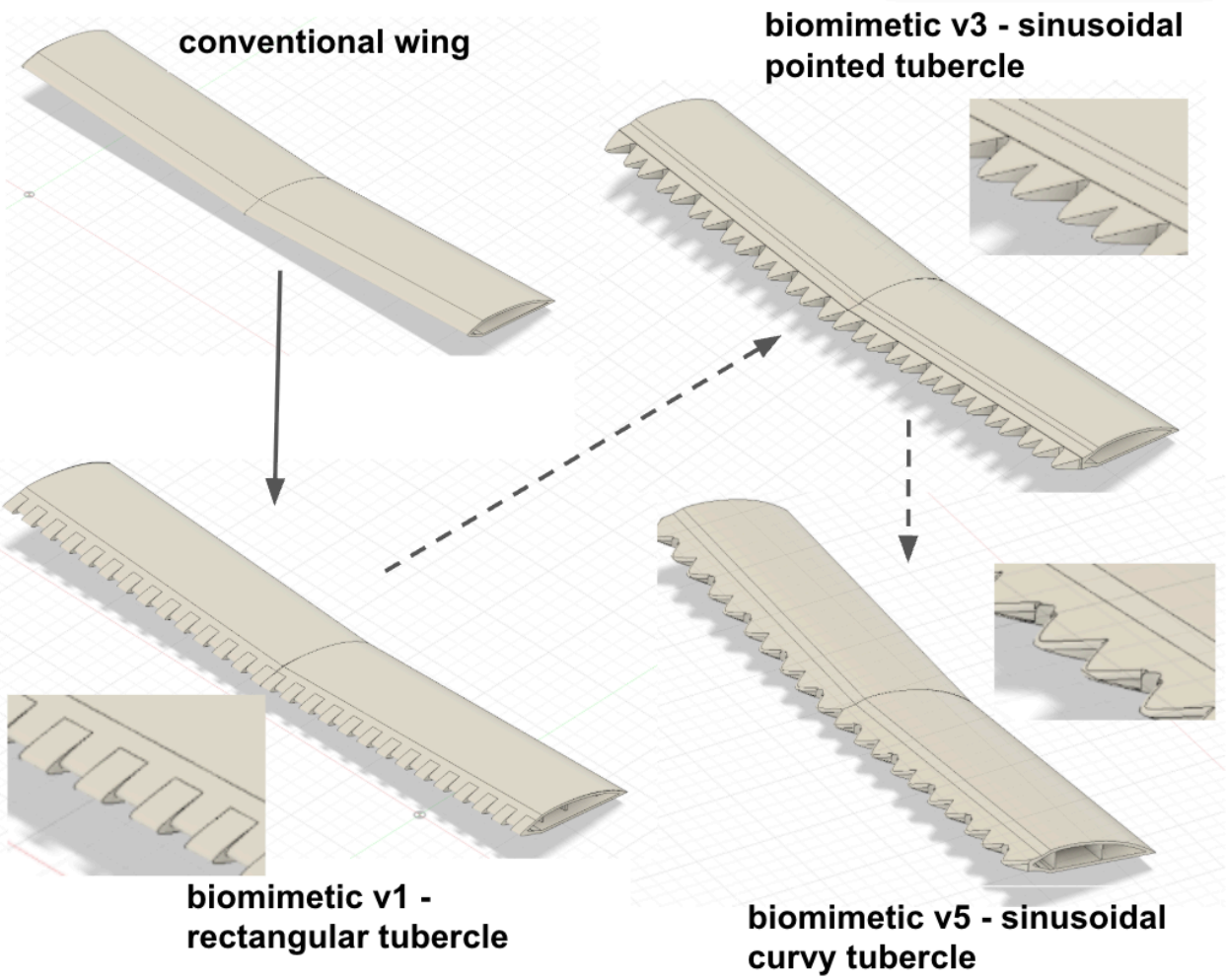

Figure 5. 3D CAD models of the full-wing Phase 2 designs. (A) The conventional full-wing. (B) Multiple versions of the whale-mimetic full-wing. These designs were used for CFD, wind-tunnel testing, and flight testing on the custom-built prototype aircraft.

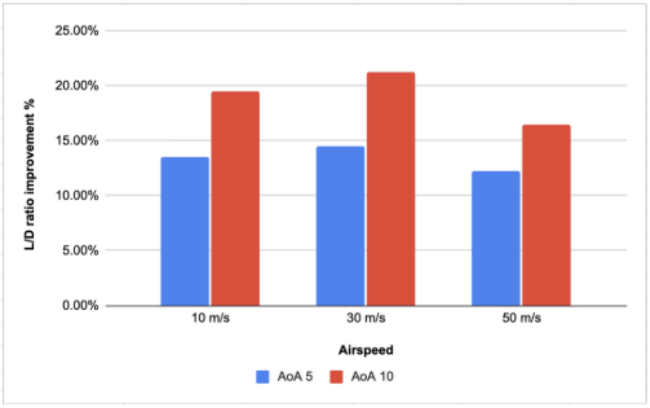

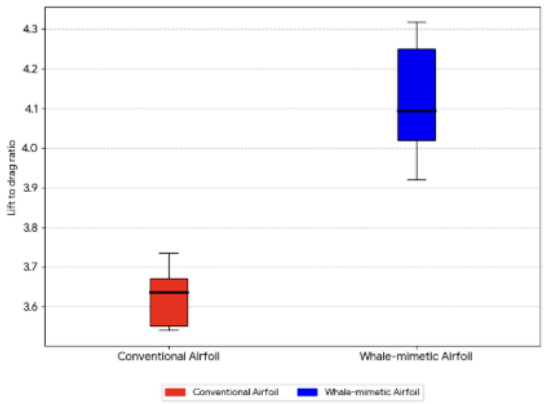

This preprint reports new research that has not been peer-reviewed and revised at the time of posting.

Figure 6. Improvement in lift-to-drag ratio from Phase 2 CFD simulations on full-wing models. (A) Bar chart illustrating the percentage improvement in the lift-to-drag (L/D) ratio of biomimetic wings compared to conventional wings (n=30). Simulations confirmed improvements in the lift-to-drag ratio for the whale-mimetic model relative to the conventional model. Improvements peaked at approximately 21% at a 10-degree AoA and a wind speed of 30 m/s. The improvement was around 12% to 14.5% at the airspeeds tested at a 5-degree AoA. Consistent improvements were observed across all simulated angles and airspeeds. (B) Box-and-whisker plot comparing the absolute L/D ratios of conventional and biomimetic wings at a 5° AoA and an airspeed of 10 m/s. The biomimetic wing demonstrated a significantly higher L/D ratio (Two-sample t-test, $p = 0.00049$). We can be 95% confident that the mean difference in the lift-to-drag ratio between the whale-mimetic and conventional aerofoils at an angle of attack of 5 and an airspeed of 10 m/s is from 0.2928 to 0.6935.

Wing Type	Average Speed (meter/second)	Max Altitude (feet)	Average Dist / Volt (meter/Volt)
Conventional	**10.33**	**124**	**1596.90**
Whale-mimetic	**9.9**	**127**	**1802.01**

Table 1: Flight Test results summary. Meter per Volt (m/V) efficiency results derived from filtered telemetry data indicated efficiency improvements of approximately 12% for the 40.5-inch whale-mimetic full-wing relative to the conventional full-wing. Efficiency gains are similar to those observed in the CFD simulations.

This preprint reports new research that has not
been peer-reviewed and revised at the time of posting.

CC BY